3D phase-sensitive inversion recovery sequence for intracranial vertebrobasilar artery dissection

Authors:

Takuya Enoki[a, b, 1], Katsuhiro Kida[a], Wataru Jomoto[b], Yusuke Kawanaka[c], Manabu Shirakawa[d], Masataka Miyama[d, 2], Noriko Kotoura[b], Sachiko Goto[a]

Author affiliations:

[a]Graduate School of Health Sciences, Okayama University, 2-5-1, Shikata-cho, Kita-ku, Okayama 700-8558, Japan

[b]Department of Radiological Technology, Hyogo Medical University Hospital, 1-1, Mukogawa-cho, Nishinomiya-shi, Hyogo 663-8501, Japan

[c]Department of Radiology, Hyogo Medical University, 1-1, Mukogawa-cho, Nishinomiya-shi, Hyogo 663-8501, Japan

[d]Department of Nuerosurgery, Hyogo Medical University, 1-1, Mukogawa-cho, Nishinomiya-shi, Hyogo 663-8501, Japan

Present address

[1]Department of Radiological Technology, Hyogo Medical University Hospital Sasayama Medical Center, 5, Kurooka, Tambasasayama-shi, Hyogo 669-2321, Japan

[2]Department of Neurosurgery, Takarazuka City Hospital, 4-5-1, Kohama, Takarazuka-shi, Hyogo 665-0827, Japan

E-mail

Takuya Enoki:

Katsuhiro Kida: kida-katsu@okayama-u.ac.jp

Wataru Jomoto: wataru-j@hyo-med.ac.jp

Yusuke Kawanaka: y-kawa@hyo-med.ac.jp

Manabu Shirakawa: mana-ns@hyo-med.ac.jp

Masataka Miyama: ng.miyama1003@gmail.com

Noriko Kotoura: rt4562@hyo-med.ac.jp

Sachiko Goto: goto@md.okayama-u.ac.jp

Corresponding author:

Katsuhiro Kida

Graduate School of Health Sciences, Okayama University, 2-5-1, Shikata-cho, Kita-ku, Okayama 700-8558, Japan

E-mail: kida-katsu@okayama-u.ac.jp

Tel: +81-86-235-6876

Fax: +81-86-222-3717

Funding:

This research did not receive any specific grant from funding agencies in the public, commercial, or not-for-profit sectors.

Declaration of interest: none

Highlights

- T1W-3D-TSE with variable refocusing flip angles are used to diagnose iVAD.
- Susceptibility artifacts of the cavernous sinus may cause vessel wall defects.
- 3D PSIR reconstructs images while maintaining signal polarity through phase correction.
- 3D-PSIR improved the vessel wall defects caused by the susceptibility artifacts.
- 3D-PSIR achieved MRI findings comparable to those of the T1W-3D-TSE in iVAD.

Abstract

Background: T1-weighted 3D turbo spin echo (T1W-3D-TSE) sequences with variable refocusing flip angle are commonly used to diagnose intracranial vertebrobasilar artery dissection (iVAD). However, magnetic susceptibility artifacts of the cavernous sinus may cause loss of the basilar and vertebral arteries. This study investigated the effectiveness of a 3D phase-sensitive inversion recovery (3D-PSIR) sequence in reducing magnetic susceptibility artifacts in the cavernous sinus, and its imaging findings for iVAD.

Methods: Twelve volunteers and eleven patients with iVAD were included. Magnetic resonance imaging (MRI) was performed using a 3.0-T MRI system. 3D-PSIR and T1W-3D-TSE sequences were used. Vessel wall defects and contrast-to-noise ratio (CNR) were evaluated. The MRI findings were visually evaluated.

Results: In the 3D-PSIR images, one volunteer (8%) had vessel wall defects, and five (42%) had vessel wall defects (p =0.046) in the T1W-3D-TSE images. CNR was higher in 3D-PSIR images for vessel wall-to-lumen, whereas it was higher in T1W-3D-TSE images for vessel wall-to-CSF (p <0.001). Visual evaluation revealed similar MRI findings between the two sequences.

Conclusions: The 3D-PSIR sequence was able to improve the vessel wall defects and achieve MRI findings comparable to those of the T1W-3D-TSE sequence in iVAD. The 3D-PSIR sequence can be a useful tool for the imaging-based diagnosis of iVAD.

Keywords: Phase sensitive inversion recovery; intracranial vertebrobasilar artery dissection; Magnetic resonance imaging; Brain

1 Introduction

Intracranial vertebrobasilar artery dissection (iVAD) is one of the most common etiologies of stroke in young to middle-aged patients [1,2], and iVAD is more frequent in East Asian countries than in Western ones [3]. An arterial intima tear triggers iVAD and the formation of intramural hematoma (IMH) and false lumen [1,4]; sudden severe headache and neck pain are the most common symptoms [1]. As iVAD can cause subarachnoid hemorrhage or cerebral infarction [1,5], accurate diagnosis is important to determine treatment options.

Typical magnetic resonance imaging (MRI) findings in iVAD include double lumen/intimal flap, IMH, luminal stenosis, and aneurysmal dilatation [6]. IMH in the subacute to early chronic stage is an important finding of iVAD, which is depicted by hyperintensity on T1-weighted (T1W) vessel wall imaging (VWI) on MRI [7–10]. Ahn et al. reported that iVAD with confirmed IMH showed approximately four times more disease progression than that without IMH [10]. VWI requires suppression of the luminal blood signal to evaluate the vessel wall; 3D turbo spin echo (TSE) with variable refocusing flip angle (VRFA) is a typical imaging method for VWI [11,12]. By setting the imaging slab of T1W-3D-TSE parallel to the vertebrobasilar artery, a wide area can be delineated, and any cross-section can be reconstructed for the vessel [11]. Furthermore, blood suppression can be improved by using an improved motion-sensitized driven equilibrium (iMSDE) preparation [13]. However, the magnetic susceptibility artifact of the cavernous sinus may cause partial signal loss in the basilar and vertebral arteries.

3D phase-sensitive inversion recovery (PSIR) is an imaging sequence with a blood suppression effect by inversion recovery (IR) pulses, and can reconstruct a real

image in which signal polarity is maintained by phase correction [14]. 3D-PSIR is not only sensitive to intraplaque hemorrhage of the carotid artery [14–16], but also to IMH of the carotid dissection [17]. Here, we focus on the possibility that the phase correction of 3D-PSIR might reduce susceptibility artifacts. It would be clinically useful if 3D-PSIR could delineate the areas of signal loss in T1W-3D-TSE by phase correction. This study aimed to apply 3D-PSIR to iVAD and to verify its effectiveness in reducing magnetic susceptibility artifacts in the cavernous sinus and its imaging findings for iVAD.

2 Methods

2.1 Participants

Twelve volunteers (6 men and 6 women; age range, 25–54 years; mean age, 37.8 years) were included in the study. For the pilot study, eleven patients (6 men and 5 women; age range, 30–78 years; mean age, 59.4 years) diagnosed with iVAD from October 2022 to September 2023 were included. The Institutional Review Board of Hyogo Medical University approved (approval number 202206-070) this study, and informed consent was obtained from all participants in accordance with the Declaration of Helsinki.

2.2 Imaging protocol

MRI scans were acquired using a 3.0-T MRI system with a 32-channel phased-array head coil (Ingenia; Philips Healthcare, Best, Netherlands). 3D time-of-flight (TOF) MR angiography (MRA) was obtained and used as a reference image for VWI. The imaging planes of 3D-PSIR and T1W-3D-TSE were oblique coronal parallel to the vertebrobasilar artery. PSIR was performed using a 3D turbo field echo (TFE) sequence. The imaging

parameters were as follows: field of view, 167 mm; voxel size, 0.8 mm × 0.8 mm × 0.7 mm; number of slices, 90; number of excitations, 1; sensitivity encoding factor, 1.5; profile order, low high-radial; TFE factor, 35; shot interval, 1,100 ms; repetition time (TR), 10 ms; echo time (TE), 4.6 ms; inversion time, 420 ms; flip angle (FA), 15°; PSIR FA, 15°; fat suppression, spectrally adiabatic inversion recovery; bandwidth (BW), 289 Hz/pixel; and scan time, 6 min 32 s. T1W-3D-TSE was performed using a VRFA and iMSDE preparation. The imaging parameters were as follows: field of view, 156 mm; voxel size, 0.7 mm × 0.7 mm × 0.7 mm; number of slices, 90; number of excitations, 1; sensitivity encoding factor, 1.5; profile order, low high-radial; TSE factor, 25; TR, 650 ms; TE, 16 ms; refocusing control angle, 50°; fat suppression, spectrally adiabatic inversion recovery; BW, 243 Hz/pixel; and scan time, 5 min 11 s.

2.3 Volunteer study

All data were transferred to the IntelliSpace Portal (version 8; Philips). 3D-PSIR and T1W-3D-TSE were reconstructed in the workstation with an axial section perpendicular to the vertebrobasilar artery at a 1-mm slice thickness. First, the presence of vessel wall defects due to magnetic susceptibility artifacts in the cavernous sinus was evaluated for both sequences. Next, the contrast-to-noise-ratio (CNR) between the vessel wall and vessel lumen and between the vessel wall and cerebrospinal fluid (CSF) in the reconstructed images was determined using the following equations:

$$CNR_{wall\ to\ lumen}=|S_{wall}-S_{lumen}|/SD_{brainstem}, \quad (1)$$

$$CNR_{wall\ to\ CSF}=|S_{wall}-S_{CSF}|/SD_{brainstem}, \quad (2)$$

where S_{wall} is the signal intensity of the vessel wall, S_{lumen} is the signal intensity of the

vessel lumen, S_{CSF} is the signal intensity of the CSF, and $SD_{brainstem}$ is the standard deviation (SD) of the signal intensity of the brainstem. A region of interest (ROI) of ≥40 mm^2 was set in the brainstem to prevent the effects of inhomogeneous noise distribution due to parallel imaging [18,19].

2.4 Patient study

A qualitative evaluation was performed as a pilot study to validate the MRI findings of iVADs observed in 3D-PSIR. Two experienced radiologists (Y. K. and Y. F.) and one experienced neurosurgeon (M. S.), who were blinded to the patient information, performed a visual evaluation of the following four MRI findings in 3D-PSIR and T1W-3D-TSE: (1) double lumen/intimal flap, (2) IMH, (3) luminal stenosis, and (4) aneurysmal dilatation [11]. The certainty of the MRI findings was rated on a 4-point scale as follows: 1 = not present, 2 = probably not present, 3 = probably suspicious, and 4 = strongly suspicious. The images of the two sequences were evaluated individually. Maximum intensity projection (MIP) images of MRA were used to identify the lesions. 3D-PSIR and T1W-3D-TSE were displayed by multiplanar reconstruction (MPR), allowing the evaluator to observe any cross-section. The window level and width could be freely adjusted by the evaluator.

2.5 Statistical analysis

Differences in the rates of vessel wall defects between 3D-PSIR and T1W-3D-TSE were evaluated using the McNemar test. Wilcoxon's signed-rank test was used to evaluate the CNR of 3D-PSIR and T1W-3D-TSE. Statistical analysis was performed using the JMP

Pro ver.15.2.0 software (SAS Institute, Cary, NC, USA). Statistical significance was set at p <0.05.

3 Results

Table 1 shows the number and rate of vessel wall defects in the 3D-PSIR and T1W-3D-TSE images. One volunteer (8%) had vessel wall defects in 3D-PSIR; whereas, in T1W-3D-TSE, five volunteers (42%) had vessel wall defects (p =0.046). One volunteer with vessel wall defects in 3D-PSIR also had vessel wall defects in T1W-3D-TSE. Figure 1 shows a representative case of 3D-PSIR and T1W-3D-TSE images of a volunteer. On the T1W-3D-TSE image, the vessel wall had a defect; however, it was depicted on the 3D-PSIR image. Figure 2 shows a representative case of the vessel wall defect in the 3D-PSIR images. The 3D-PSIR image shows a partial defect in the vessel wall, whereas the T1W-3D-TSE image shows a comparatively greater defect in the vessel wall.

Figure 3 shows the CNR results for 3D-PSIR and T1W-3D-TSE images. The median $CNR_{wall\ to\ lumen}$ for 3D-PSIR and T1W-3D-TSE images were 18.65 [15.49–20.63] and 5.68 [4.93–6.41], respectively, with 3D-PSIR images showing significantly higher values than T1W-3D-TSE ones (p <0.001). The median $CNR_{wall\ to\ CSF}$ for 3D-PSIR and T1W-3D-TSE images were 0.55 [0.23–0.96] and 2.45 [1.83–2.92], respectively, with T1W-3D-TSE images showing significantly higher values than 3D-PSIR ones (p <0.001).

Table 2 presents the results of the visual evaluation. The scores shown in the table are the averages of the three evaluators. Except for the following six instances, the scores for the four MRI findings were similar between the 3D-PSIR and T1W-3D-TSE images. In the MRI findings of patient 2, the score for the double lumen/intimal flap was

4 for the 3D-PSIR image and 1.7 for the T1W-3D-TSE image. For patient 4, the score for the double lumen/intimal flap was 1.7 on the 3D-PSIR image and 3.7 on the T1W-3D-TSE image. Regarding the MRI findings of IMH in patient 4, the score was 3.7 on the 3D-PSIR image and 1.3 on the T1W-3D-TSE image. For patient 6, the score for aneurysmal dilatation was 3.0 on the 3D-PSIR image and 2.0 on the T1W-3D-TSE image. For patient 9, the score for the double lumen/intimal flap was 2.0 on the 3D-PSIR image and 3.7 on the T1W-3D-TSE image. Regarding the MRI findings of aneurysmal dilatation in patient 9, the score was 4.0 on the 3D-PSIR image and 2.3 on the T1W-3D-TSE image.

Figure 4 shows a case of left vertebral artery dissection in patient 1. The lesion showed IMH, luminal stenosis, and aneurysmal dilatation. IMH was visualized on both T1W-3D-TSE and 3D-PSIR images. Figure 5 shows a case of right vertebral artery dissection in patient 2. The lesion exhibited intimal flap, IMH, and aneurysmal dilatation. The intimal flap was visualized on the 3D-PSIR image, surpassing its visibility on T1W-3D-TSE.

4 Discussion

Our study demonstrated that 3D-PSIR improves vessel wall defects caused by susceptibility artifacts in the cavernous sinus. Furthermore, a pilot study confirmed that 3D-PSIR is a promising imaging technique for iVAD diagnosis.

Compared to T1W-3D-TSE, 3D-PSIR demonstrated an approximately 80% improvement in vessel wall defects caused by susceptibility artifacts in the cavernous sinus. The 3D-PSIR image is reconstructed correcting for phase errors, and the effectiveness of this phase correction has been demonstrated. Phase errors are influenced

by various factors, including magnetic susceptibility variations, receiver resonance offset, phase associated with the B_1 field, eddy currents, gradient group delays, mismatches of frequency-encoding gradient and data acquisition window timing, as well as motion and flow [20]. We believe that, in this study, phase errors caused by changes in magnetization were effectively corrected. However, complete artifact correction has not been achieved, indicating the limitations of phase correction. T1W-3D-TSE is a spin-echo-based sequence that is generally considered to be less affected by magnetization artifacts. However, our study revealed that T1W-3D-TSE is affected by magnetic susceptibility artifacts of the cavernous sinus. To the best of our knowledge, this is the first report of its kind.

The 3D-PSIR sequence utilizes an IR pulse and achieves high T1 contrast through real reconstruction. The 3D-PSIR sequence that we employed was optimized to assign negative values to the blood and positive values to other tissues. Consequently, we believe that the contrast between the vessel lumen and vessel wall was enhanced compared to the T1W-3D-TSE images. However, the contrast between the vessel wall and CSF was reduced in comparison to the T1W-3D-TSE images, indicating the need for further improvement through additional parametric adjustments.

In the pilot study, the 3D-PSIR images demonstrated similar MRI findings as the T1W-3D-TSE ones. Therefore, we believe that the 3D-PSIR sequence is a clinically viable imaging technique for iVAD. Differences in scores for the double lumen/intimal flap were observed between the two sequences in three patients. Natori et al. reported a low sensitivity of the T1W-3D-TSE sequence for intimal flaps and considered that this might be due to the difficulty in detecting high-signal intimal flaps among low-signal

vessels [12]. A similar situation can be assumed in the present study. Additionally, the T1W-3D-TSE sequence in this study utilized iMSDE, which might have suppressed the signal of the intimal flaps by motion-sensitized gradients (MSG). However, the 3D-PSIR sequence might have lacked the ability to detect intimal flaps due to lower in-plane resolution compared to the T1W-3D-TSE sequence. In some cases, there was an increased score in the MRI findings of IMH on the 3D-PSIR sequence, indicating a higher sensitivity of the 3D-PSIR sequence towards IMH. This observation is consistent with that reported by Huang et al. [17]. There was an increased score in the MRI findings of aneurysmal dilatation on the 3D-PSIR sequence in some cases, indicating that this was due to the 3D-PSIR sequence's enhanced ability to suppress low-velocity blood flow compared to the T1W-3D-TSE sequence. Wang et al. reported that the 3D-PSIR sequence tended to show a larger lumen size compared to TOF. They speculated that this might be due to the insensitivity of the IR pulse used in 3D-PSIR to flow velocity [14]. The blood suppression effectiveness is reduced in the T1W-3D-TSE sequence owing to the slow blood flow in the proximity of the vessel wall [21]. Owing to the complex nature of blood flow in aneurysms [22], it is anticipated that the efficacy of blood suppression would be diminished in cases of aneurysmal dilatation. It can be inferred that the T1W-3D-TSE sequence employing MSG for blood suppression cannot completely inhibit the slow flow of blood in the proximity of the vessel wall. Conversely, the 3D-PSIR sequence achieves effective blood suppression even in the proximity of the vessel wall, which may contribute to a higher score in cases of aneurysmal dilatation.

This study had several limitations. First, the recruitment period for patients was relatively short, resulting in an inadequate number of cases. Although the pilot study

confirmed that the MRI findings of the 3D-PSIR sequence were acceptable for iVAD, these findings need to be confirmed in more cases. Second, there was a lack of cases where artifacts appeared in the lesion area. Although it was evident that the artifacts improved in volunteer studies, confirmation through clinical cases is necessary.

5 Conclusion

The 3D-PSIR sequence may be able to improve the vessel wall defects caused by artifacts in the cavernous sinus and achieve MRI findings comparable to those of the T1W-3D-TSE sequence in iVAD. 3D-PSIR can, therefore, be a useful tool for the imaging-based diagnosis of iVAD.

Acknowledgements:

We would like to thank Editage (www.editage.jp) for English language editing.

References

[1] Schievink WI. Spontaneous dissection of the carotid and vertebral arteries. N Engl J Med 2001;344:898–906. https://doi.org/10.1056/NEJM200103223441206.

[2] Schievink WI, Mokri B, O'Fallon WM. Recurrent spontaneous cervical-artery dissection. N Engl J Med 1994;330:393–7. https://doi.org/10.1056/NEJM199402103300604.

[3] Kim BM, Kim SH, Kim DI, Shin YS, Suh SH, Kim DJ et al. Outcomes and prognostic factors of intracranial unruptured vertebrobasilar artery dissection. Neurology 2011;76:1735–41. https://doi.org/10.1212/WNL.0b013e31821a7d94.

[4] Keser Z, Meschia JF, Lanzino G. Craniocervical artery dissections: A concise review for clinicians. Mayo Clin Proc 2022;97:777–83. https://doi.org/10.1016/j.mayocp.2022.02.007.

[5] Arnold M, Bousser M. Clinical manifestations of vertebral artery dissection. Front Neurol Neurosci 2005;20:77–86. https://doi.org/10.1159/000088152.

[6] Choi YJ, Jung SC, Lee DH. Vessel wall imaging of the intracranial and cervical carotid arteries. J Stroke 2015;17:238–55. https://doi.org/10.5853/jos.2015.17.3.238.

[7] Iwama T, Andoh T, Sakai N, Iwata T, Hirata T, Yamada H. Dissecting and fusiform aneurysms of vertebro-basilar systems. MR imaging. Neuroradiology 1990;32:272–9. https://doi.org/10.1007/BF00593045.

[8] Kitanaka C, Tanaka J, Kuwahara M, Teraoka A. Magnetic resonance imaging study of intracranial vertebrobasilar artery dissections. Stroke 1994;25:571–5. https://doi.org/10.1161/01.str.25.3.571.

[9] Hosoya T, Adachi M, Yamaguchi K, Haku T, Kayama T, Kato T. Clinical and neuroradiological features of intracranial vertebrobasilar artery dissection. Stroke 1999;30:1083–90. https://doi.org/10.1161/01.str.30.5.1083.

[10] Ahn SS, Kim BM, Suh SH, Kim DJ, Kim DI, Shin YS et al. Spontaneous symptomatic intracranial vertebrobasilar dissection: initial and follow-up imaging findings. Radiology 2012;264:196–202. https://doi.org/10.1148/radiol.12112331.

[11] Mandell DM, Mossa-Basha M, Qiao Y, Hess CP, Hui F, Matouk C et al. Intracranial vessel wall MRI: principles and expert consensus recommendations of the American Society of Neuroradiology. AJNR Am J Neuroradiol 2017;38:218–29. https://doi.org/10.3174/ajnr.A4893.

[12] Natori T, Sasaki M, Miyoshi M, Ohba H, Oura MY, Narumi S et al. Detection of vessel wall lesions in spontaneous symptomatic vertebrobasilar artery dissection using T1-weighted 3-dimensional imaging. J Stroke Cerebrovasc Dis 2014;23:2419–24. https://doi.org/10.1016/j.jstrokecerebrovasdis.2014.05.019.

[13] Wang J, Yarnykh VL, Yuan C. Enhanced image quality in black-blood MRI using the improved motion-sensitized driven-equilibrium (iMSDE) sequence. J Magn Reson Imaging 2010;31:1256–63. https://doi.org/10.1002/jmri.22149.

[14] Wang J, Börnert P, Zhao H, Hippe DS, Zhao X, Balu N et al. Simultaneous noncontrast angiography and intraplaque hemorrhage (SNAP) imaging for carotid atherosclerotic disease evaluation. Magn Reson Med 2013;69:337–45. https://doi.org/10.1002/mrm.24254.

[15] Fujiwara Y, Mio M. Improvement in the contrast-to-noise ratio and quantitative measurement of T1 and T2* values for carotid atherosclerotic plaque using multi-echo phase-sensitive inversion recovery. Radiol Phys Technol 2021;14:186–92. https://doi.org/10.1007/s12194-021-00619-1.

[16] Zhou Z, Li R, Zhao X, He L, Wang X, Wang J et al. Evaluation of 3D multi-contrast joint intra- and extracranial vessel wall cardiovascular magnetic resonance. J Cardiovasc Magn Reson 2015;17:41. https://doi.org/10.1186/s12968-015-0143-z.

[17] Huang RJ, Lu Y, Zhu M, Zhu JF, Li YG. Simultaneous non-contrast angiography and intraplaque haemorrhage (SNAP) imaging for cervical artery dissections. Clin Radiol 2019;74:817.e1–7. https://doi.org/10.1016/j.crad.2019.06.018.

[18] Heverhagen JT. Noise measurement and estimation in MR imaging experiments. Radiology 2007;245:638–9. https://doi.org/10.1148/radiol.2453062151.

[19] Qiao Y, Steinman DA, Qin Q, Etesami M, Schär M, Astor BC et al. Intracranial arterial wall imaging using three-dimensional high isotropic resolution black blood MRI at 3.0 Tesla. J Magn Reson Imaging. 2011;34:22–30. https://doi.org/10.1002/jmri.22592.

[20] Bernstein MA, King KF, Zhou XJ. Handbook of MRI pulse sequences; 2004, p. 616–22.

[21] Lindenholz A, van der Kolk AG, Zwanenburg JJM, Hendrikse J. The use and pitfalls of intracranial vessel wall imaging: how we do it. Radiology 2018;286:12–28. https://doi.org/10.1148/radiol.2017162096.

[22] Cornelissen BMW, Leemans EL, Coolen BF, Peper ES, van den Berg R, Marquering HA et al. Insufficient slow-flow suppression mimicking aneurysm wall enhancement in magnetic resonance vessel wall imaging: a phantom study. Neurosurg Focus 2019;47:E19. https://doi.org/10.3171/2019.4.FOCUS19235.

Legends

Table 1

Results of vessel wall defects in 3D-PSIR and T1W-3D-TSE

Table 2

Results of the visual evaluation

Figure 1

Representative case of 3D-PSIR and T1W-3D-TSE images of a volunteer. (a) 3D-PSIR

image of the basilar artery level. (b) T1W-3D-TSE image of the basilar artery level. (c) 3D-PSIR images of the vertebral artery level. (d) T1W-3D-TSE image of the vertebral artery level. At the vertebral artery level, the vessel wall is delineated in both the 3D-PSIR and T1W-3D-TSE sequences (arrowhead); however, at the basilar artery level, the vessel wall defect can be observed in T1W-3D-TSE (arrow). 3D-PSIR: three-dimensional phase-sensitive inversion recovery; T1W-3D-TSE: T1-weighted three-dimensional turbo spin echo.

Figure 2

Representative case of a vessel wall defect in 3D-PSIR and T1W-3D-TSE images. (a)3D-PSIR image. (b)T1W-3D-TSE image. A larger area of the vessel wall is deficient in the T1W-3D-TSE image (arrowhead) compared to 3D-PSIR image (arrow). 3D-PSIR: three-dimensional phase-sensitive inversion recovery; T1W-3D-TSE: T1-weighted three-dimensional turbo spin echo.

Figure 3

CNR for the 3D-PSIR and T1W-3D-TSE images. (a) $CNR_{wall\ to\ lumen}$ is significantly higher for the 3D-PSIR images than for the T1W-3D-TSE images. (b) $CNR_{wall\ to\ CSF}$ is significantly higher for the T1W-3D-TSE images than for the 3D-PSIR images. 3D-PSIR: three-dimensional phase-sensitive inversion recovery; CNR: contrast-to-noise ratio; T1W-3D-TSE: T1-weighted three-dimensional turbo spin echo.

Figure 4

Case presentation of patient 1. (a) MRA MIP image showing iVAD with aneurysmal dilatation in the left vertebral artery (arrow). (b) 3D-PSIR coronal and (d) transverse images showing IMH as well as (c, e) T1W-3D-TSE (arrowheads). 3D-PSIR: three-dimensional phase-sensitive inversion recovery; IMH: intramural hematoma; iVAD: intracranial vertebrobasilar artery dissection; MIP: maximum intensity projection; MRA: magnetic resonance angiography; T1W-3D-TSE: T1-weighted three-dimensional turbo spin echo.

Figure 5

Case presentation of patient 2. (a) MRA MIP image showing iVAD with aneurysmal dilatation in the right vertebral artery (arrow). Coronal images of (b) 3D-PSIR and (c) T1W-3D-TSE showing aneurysmal dilatation and IMH (dashed arrows). (d) 3D-PSIR depicting an intimal flap, but (e) T1W-3D-TSE does not (arrowheads). 3D-PSIR: three-dimensional phase-sensitive inversion recovery; IMH: intramural hematoma; iVAD: intracranial vertebrobasilar artery dissection; MIP: maximum intensity projection; MRA: magnetic resonance angiography; T1W-3D-TSE: T1-weighted three-dimensional turbo spin echo.

Table 1. Results of vessel wall defects in 3D-PSIR and T1W-3D-TSE

Sequence	Wall defect, n=12
3D-PSIR	1 (8%)
T1W-3D-TSE	5 (42%)*

3D-PSIR, 3-dimensional phase sensitive inversion recovery;
T1W-3D-TSE, T1-weighted 3-dimensional turbo spine echo.
Data are presented as n (%).
*p= 0.046

Table 2. Results of the visual evaluation

Patient No.	MRI findings							
	Double lumen/intimal flap		IMH		Luminal stenosis		Aneurysmal dilatation	
	3D-PSIR	T1W-3D-TSE	3D-PSIR	T1W-3D-TSE	3D-PSIR	T1W-3D-TSE	3D-PSIR	T1W-3D-TSE
1	1.3	1.7	4	4	4	4	4	4
2	4	1.7	3.7	4	1.7	1.3	4	4
3	1.3	1.7	3.7	4	1.7	2.3	1.7	2.3
4	1.7	3.7	3.7	1.3	3	4	4	3.7
5	1.7	2	1.7	2.7	1.7	2	3.3	4
6	2	2.7	3.7	3.7	4	4	3	2
7	1.0	1.0	4.0	4.0	4.0	4.0	1.3	1.7
8	1.3	1.7	3.7	4.0	3.3	3.7	2.3	2.0
9	2.0	3.7	1.3	1.7	4.0	3.3	4.0	2.3
10	3.7	3.0	1.0	1.7	2.0	1.3	4.0	4.0
11	1.0	1.0	4.0	4.0	2.7	2.7	2.0	1.7

3D-PSIR, 3-dimensional phase sensitive inversion recovery; IMH, intramural hematoma;
T1W-3D-TSE, T1-weighted 3-dimensional turbo spine echo.

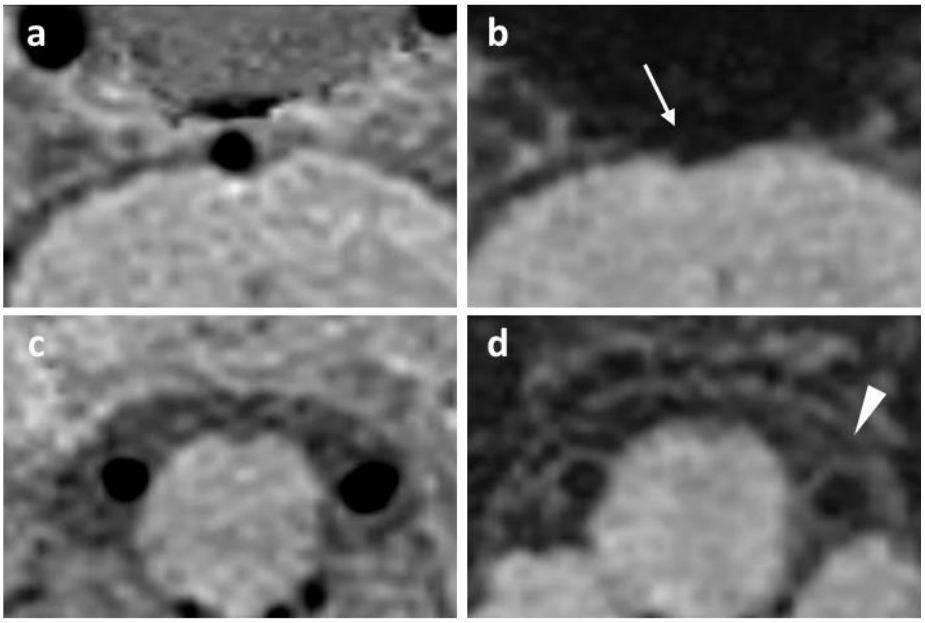

Figure 1

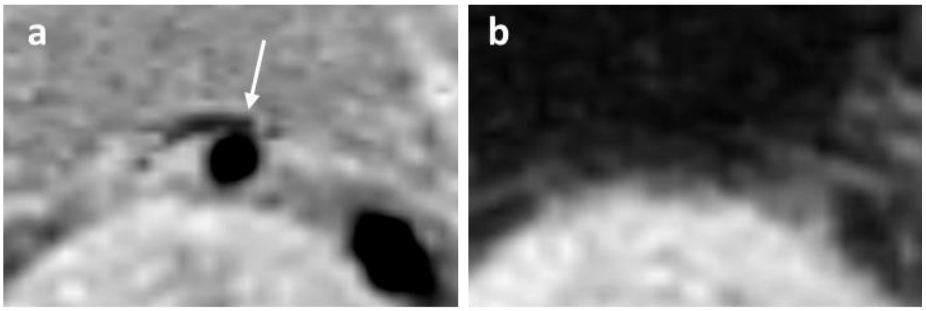

Figure 2

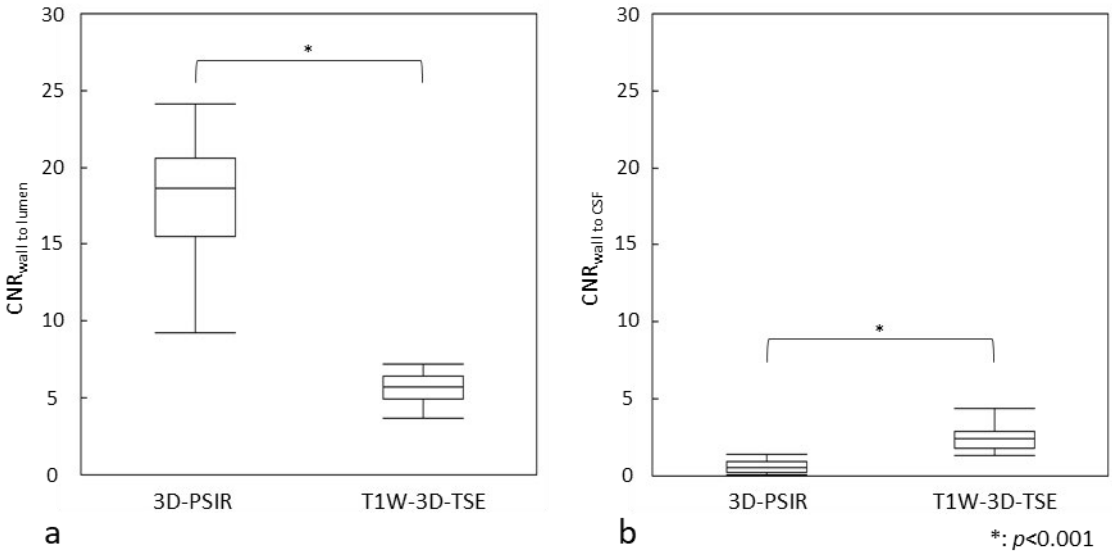

Figure 3

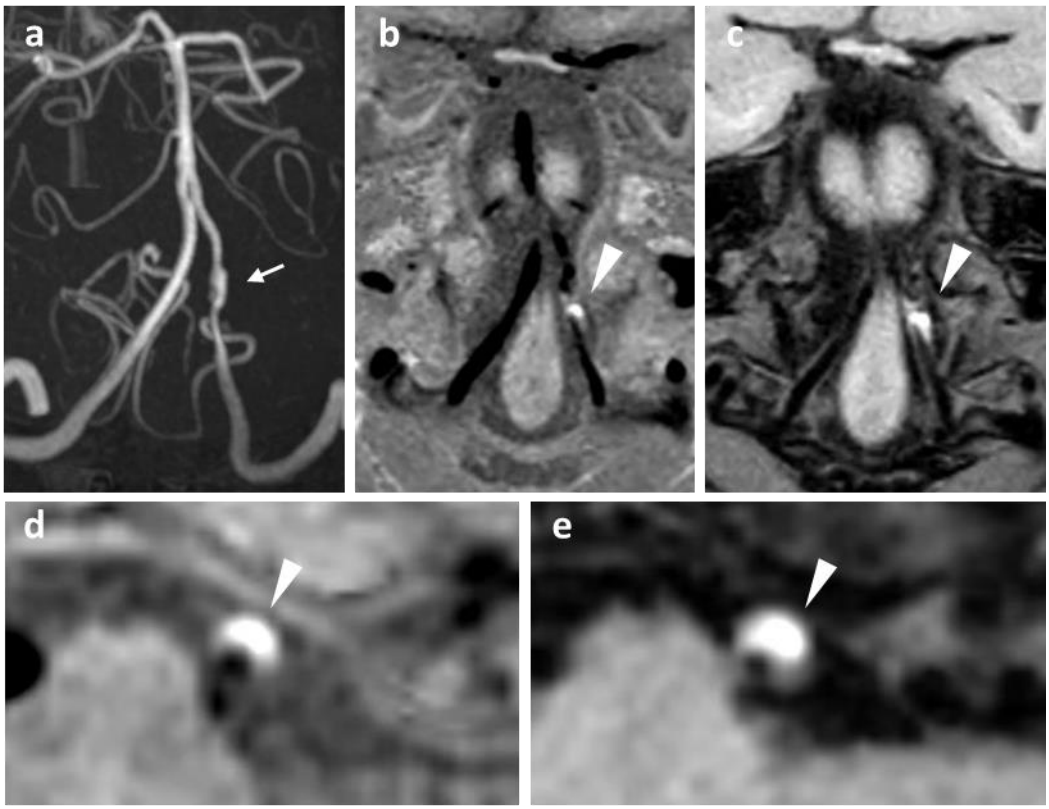

Figure 4

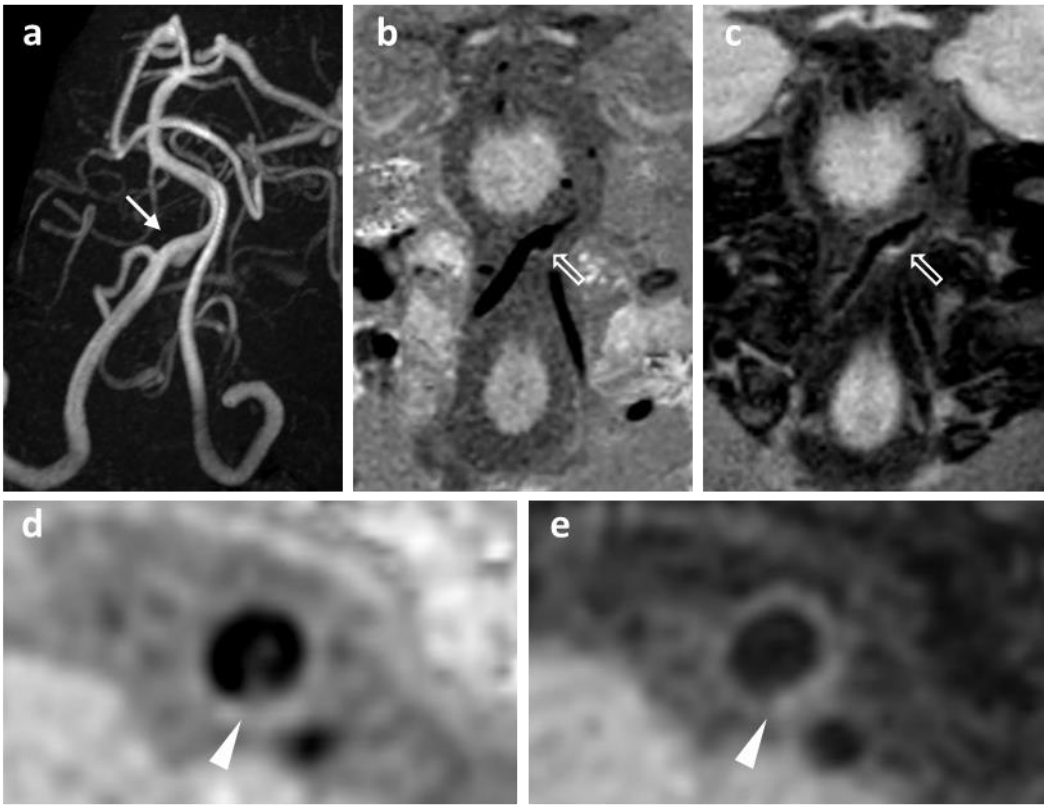

Figure 5